3210 *Chem. Mater.* **2009,** *21,* 3210–3215
DOI:10.1021/cm900702d

CHEMISTRY OF MATERIALS
Article

Sn@CNT and Sn@C@CNT nanostructures for superior reversible lithium ion storage

Yong Wang,*[,†,‡] Minghong Wu,[†] Zheng Jiao,[†] and Jim Yang Lee*[,‡]

[†]*School of Environmental and Chemical Engineering, Shanghai University, Shangda Road 99, Shanghai 200444, P. R. China, and* [‡]*Singapore-MIT Alliance, National University of Singapore, 4 Engineering Drive 4, 117576, Singapore*

Received March 12, 2009. Revised Manuscript Received May 24, 2009

In this study we demonstrate a facile templated chemical vapor deposition (CVD) method to produce CNT-encapsulated Sn nanoparticles with ~100% particle encapsulation and high filling uniformity. The encapsulated Sn particles were formed either as Sn or Sn@carbon core−shell particles with good control of size and morphology. The complete and uniform encapsulation of small, electrochemically active Sn particles within a CNT matrix with large free volume accommodated the volume excursion problem in repetitive lithium insertion and extraction reactions very well, showing good resilience in maintaining electrical connective and mechanical integrity. Consequently the completely filled Sn@CNT nanocomposite showed excellent reversible lithium ion storage properties.

Introduction

Rechargeable lithium ion batteries are now the de facto mobile power for portable electronic products. Sn-based anodes have once been suggested as a potential substitute for the graphite anode to increase the battery capacity (the theoretical gravimetric capacity of Sn at ~990 mA h g^{-1} is ~2.6 times that of graphite at 372 mA h g^{-1}).[1] However, the impressive capacity of Sn for Li storage is undermined by poor cyclability resulting from the large specific volume changes in charging and discharging. These volume changes, caused by Li−Sn alloying reaction in charging (up to a maximum of ~300% from Sn to $Li_{4.4}Sn$), and the Li−Sn dealloying reaction in discharging give rise to stress-induced electrode pulverization and the loss of electrical connectivity as a result.[1] Some of the proposed strategies to restrain the volume changes include size and morphology control of the active Sn phase and using a soft matrix (such as carbonaceous materials) to absorb the internal stress.[1−15]

A number of nanostructures have been proposed to promote lithium ion storage in tin.[2−15] Among them the hollow SnO_2 particles,[6−9] the SnO_2 nanotubes,[10−12] and the hollow carbon sphere-encapsulated Sn particles[13−15] have drawn the greatest interest. The most important feature in these materials is the void space associated with the hollow structure which allows the storage compound to expand more freely to reduce the internal stress.[6−15] Carbon nanotubes (CNTs), with their large internal cavity, high electrical conductivity, extensive surface area, and material flexibility[16,17] should be a good encapsulation matrix for the Sn particles. The majority of CNT−Sn composites reported in the literature have Sn-based particles deposited on the CNT external walls.[18,19] *There is no report on CNT-encapsulation of pristine Sn particles*. The few studies on CNT-encapsulated SnO[20] or SnO_2[21,22] all relied on capillary forces[23,24] to draw the

*Corresponding authors. E-mail: yongwang@shu.edu.cn (Y.W.), cheleejy@nus.edu.sg (J.Y.L.). Phone: +86-21-66137723. Fax: +86-21-66137725.

(1) Winter, M.; Besenhard, J. O. *Electrochim. Acta* **1999**, *45*, 31.
(2) Shin, H. C.; Liu, M. *Adv. Funct. Mater.* **2005**, *15*, 582.
(3) Derrien, G.; Hassoun, J.; Panero, S.; Scrosati, B. *Adv. Mater.* **2007**, *19*, 2336.
(4) Park, M. S.; Wang, G. X.; Kang, Y. M.; Wexler, D.; Dou, S. X.; Liu, H. K. *Angew. Chem., Int. Ed.* **2007**, *46*, 750.
(5) Todd, A. D. W.; Mar, R. E.; Dahn, J. R. *J. Electrochem. Soc.* **2007**, *154*, A597.
(6) Lee, K. T.; Lytle, J. C.; Ergang, N. S.; Oh, S. M.; Stein, A. *Adv. Funct. Mater.* **2005**, *15*, 547.
(7) Han, S. J.; Jang, B. C.; Kim, T.; Oh, S. M.; Hyeon, T. *Adv. Funct. Mater.* **2005**, *15*, 1845.
(8) Lou, X. W.; Wang, Y.; Yuan, C. L.; Lee, J. Y.; Archer, L. A. *Adv. Mater.* **2006**, *18*, 2325.
(9) Wang, Y.; Su, F. B.; Lee, J. Y.; Zhao, X. S. *Chem. Mater.* **2006**, *18*, 1347.
(10) Wang, Y.; Lee, J. Y.; Zeng, H. C. *Chem. Mater.* **2005**, *17*, 3899.
(11) Wang, Y.; Zeng, H. C.; Lee, J. Y. *Adv. Mater.* **2006**, *18*, 645.
(12) Park, M. S.; Kang, Y. M.; Wang, G. X.; Dou, S. X.; Liu, H. K. *Adv. Funct. Mater.* **2008**, *18*, 455.
(13) Lee, K. T.; Jung, Y. S.; Oh, S. M. *J. Am. Chem. Soc.* **2003**, *125*, 5652.
(14) Cui, G.; Hu, Y. S.; Zhi, L.; Wu, D.; Lieberwirth, I.; Maier, J.; Mullen, K. *Small* **2007**, *3*, 2066.
(15) Zhang, W. M.; Hu, J. S.; Guo, Y. G.; Zheng, S. F.; Zhong, L. S.; Song, W. G.; Wan, L. J. *Adv. Mater.* **2008**, *20*, 1160.
(16) Terrones, M. *Annu. Rev. Mater. Res.* **2003**, *33*, 419.
(17) Wang, Y.; Lee, J. Y. *Angew. Chem., Int. Ed.* **2006**, *45*, 7039.
(18) Wen, Z. H.; Wang, Q.; Zhang, Q.; Li, J. H. *Adv. Funct. Mater.* **2007**, *17*, 2772.
(19) Park, M. S.; Needham, S. A.; Wang, G. X.; Kang, Y. M.; Park, J. S.; Dou, S. X.; Liu, H. K. *Chem. Mater.* **2007**, *19*, 2406.
(20) Sloan, J.; Cook, J. J.; Heesom, J. R.; Green, M. L. H.; Hutchison, J. L. *J. Cryst. Growth* **1997**, *173*, 81.
(21) Zhao, L. P.; Gao, L. *Carbon* **2004**, *42*, 3269.
(22) Kumar, T. P.; Ramesh, R.; Lin, Y. Y.; Fey, G. T. K. *Electrochem. Commun.* **2004**, *6*, 520.
(23) Ajavan, P. M.; Iijima, S. *Nature* **1993**, *361*, 333.
(24) Korneva, G.; Ye, H. H.; Gogotsi, Y.; Halverson, D.; Friedman, G.; Bradley, J. C.; Kornev, K. G. *Nano Lett.* **2005**, *5*, 879.

Published on Web 06/25/2009

particle precursors into preformed CNT interiors. Such approach often experiences very low filling yield of the nanoparticles. A large number of particles still exist in isolation or are deposited on the outside walls of the CNTs,[20−22] making it difficult to obtain reliable (encapsulation) structure−property relationships.

Herein, we report a templated chemical vapor deposition (CVD) method to produce CNT-encapsulated Sn nanoparticles with ∼100% particle encapsulation and high filling uniformity. Depending on the processing conditions the encapsulated Sn nanoparticles may also be covered by a layer of carbon to form a Sn@carbon core−shell structure. These CNT encapsulated tin particles exhibited good electrochemical performance when tested as the anode for rechargeable lithium ion batteries.

Experimental Section

Materials synthesis. A porous alumina membrane (Whatman, Anodisc, 200 nm) was immersed in water for 30 min under vacuum to remove the air bubbles in the pores and then equilibrated in 0.4 M $SnCl_4$ (Riedel-de Haen, 99%) aqueous solution for 5 h, followed by oven drying at 70 °C for 5 h (Sample A). The evaporation of water from the impregnated membrane resulted in the formation of a thin liquid film of $SnCl_4$ (melting point: −33 °C) on the walls. Partial hydrolysis of $SnCl_4$ could also have taken place during drying. Sample B was similarly prepared by impregnating the alumina membrane with 1.0 M $SnCl_4$. The alumina membrane was then placed with their pores horizontally and heated in a tubular furnace where a mixture of 10% C_2H_2 and 90% N_2 flowed for 3 h at 200 sccm and 650 °C. The furnace was then cooled naturally in the gas mixture to room temperature. The upper surface of the membrane was polished gently with a sand paper (2500 grit) to remove the carbon layer before the membrane was dissolved in aqueous NaOH solution, followed by copious washing with water, centrifuging at 5000 rpm, and drying in vacuum at 130 °C for 3 h. The insoluble was recovered as the product.

Materials Characterizations. The CNT-encapsulated Sn particles (Sample A and Sample B) were characterized by field-emission scanning electron microscopy (FE-SEM), energy dispersive X-ray spectroscopy (FESEM/EDX, JEOL JSM-6700F), transmission electron microscopy (TEM), selected area electron diffraction (TEM/SAED, JEOL JSM-2010F or Philips FEG-CM300), and powder X-ray diffraction (XRD, Shimadzu XRD-6000, Cu Kα radiation).

Electrochemical Measurements. An N-methyl pyrrolidinone (NMP) slurry consisting of 80 wt % of the composite powder (CNT-encapsulated Sn particles) and 10 wt % each of carbon black (Super-P) and polyvinylidene fluoride (Aldrich) was uniformly applied to a 0.7 mm copper foil (loading of active materials: $\sim$1 mg·cm^{-2}). The coated foil was cut into disk electrodes 11 mm in diameter. The electrodes were vacuum-dried overnight at 130 °C followed by compaction at 2.0×10^6 Pa. They were then assembled into Li test cells using 0.75 mm lithium foil as the negative electrode, microporous polypropylene separator, and an electrolyte of 1 M $LiPF_6$ in a 50:50 (w/w) mixture of ethylene carbonate (EC) and diethyl carbonate (DEC). Cell assembly was carried out in a recirculating argon glovebox where both the moisture and oxygen contents were below 1 ppm each. All cells were tested galvanostatically at 0.1 mA·cm^{-2} ($\sim$100 mA·g^{-1}) and were discharged (Li^+ insertion) and charged (Li^+ extraction) between fixed voltage limits (3 V−5 mV).

Results and Discussion

CNT-encapsulated Sn nanoparticles were prepared by chemical vapor deposition (CVD) over anodized aluminum oxide (AAO) hard templates. Powder X-ray diffraction (XRD, Figure 1) disclosed that $SnCl_4$ was reduced to Sn by C_2H_2 in both Sample A (prepared from 0.4 M $SnCl_4$ aqueous solution) and Sample B (prepared from 1 M $SnCl_4$ aqueous solution). The Sn in the tin−carbon composites prepared as such were in tetragonal symmetry with lattice constants $a_0 = 5.83$ Å and $c_0 = 3.18$ Å (JCPDS 04-0673). Inductively coupled plasma (ICP) spectroscopy and elemental analysis measured the Sn contents to be 37.6 wt % for Sample A and 86.5 wt % for Sample B. The FE-SEM images of Sample A (Figure 2a,b) show arrays of carbon nanotubes with length of ∼30 μm and diameters in the range of 180−280 nm. Some of the CNT diameters were larger than the nominal pore size of the AAO template (200 nm) because of the nonuniform pore distribution in the latter. The CNTs were formed by the catalytic action of the alumina walls on C_2H_2 decomposition.[11,25] As shown in the 15 kV high-magnification FE-SEM image of Figure 2b, the Sn nanoparticles were all uniformly dispersed and exclusively contained by the CNT matrix. In this case the CNT skin was thin enough to allow the FE-SEM imaging of the encapsulated tin particles. TEM images (Figures 2c,d) found likewise the uniform dispersion of ∼6−10 nm Sn particles in ∼5−10 nm thick CNTs with no Sn nanoparticles on the exterior walls. The degree of encapsulation was therefore very high, approaching 100%. The HRTEM image in Figure 2e, besides confirming the embedment of the Sn particles within the CNT shell and on the inside walls, also reveals that the carbon shell was made up of staggered, shortened graphene sheets, which should facilitate Li-ion diffusion in and out of the Sn nanoparticle filler.[26]

The FE-SEM and TEM images of Sample B in Figure 3a−d show CNTs of the same diameters and lengths as those in Sample A. While the Sn nanoparticles were bigger (∼50−170 nm), they were still completely contained by the CNTs (FE-SEM images of Figure 3a,b and TEM image of Figure 3c,d). After rupturing the CNTs with a sand paper, a few particles could be found outside of the ruptured tips of the CNTs, but many particles were still retained by the CNTs (FE-SEM images of Figure 3e,f). The selected area electron diffraction (SAED) pattern in the inset of Figure 3c shows continuous rings which could be indexed to metallic Sn. Highlighted by the arrows in the TEM image of Figure 3d is the common feature of a ∼3−10 nm thick carbon layer on the Sn nanoparticles, forming a Sn@carbon core−shell nanostructure. This thin carbon shell on the Sn particles could improve the electrical contact between the Sn particles while resisting the agglomeration of Sn particles during cycling, a known cause for poor cyclability. The carbon overlayer was not visible in the HRTEM image

(25) Che, G.; Lakshmi, B. B.; Fisher, E. R.; Martin, C. R. *Nature* **1998**, *393*, 346.
(26) Zheng, T.; Xue, J. S.; Dahn, J. R. *Chem. Mater.* **1996**, *8*, 389.

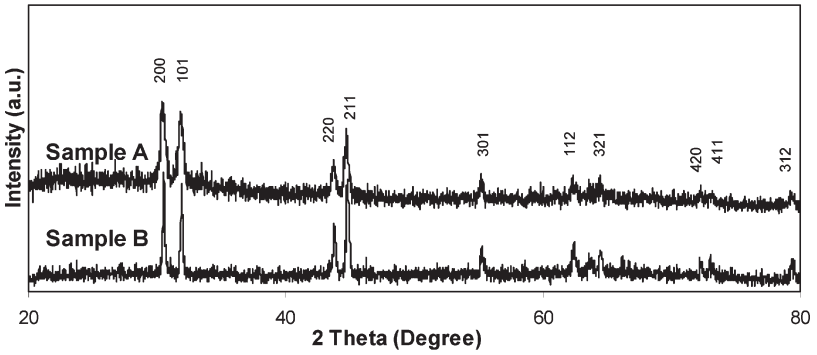

Figure 1. Powder X-ray diffraction pattern (XRD) of CNT-encapsulated Sn nanoparticles prepared from aqueous $SnCl_4$ solutions (Sn@CNT, Sample A: 0.4 M $SnCl_4$ and Sn@C@CNT, Sample B: 1 M $SnCl_4$). All peaks could be indexed to tetragonal Sn (JCPDS 04-0673). The diffraction peaks of CNTs were not found by XRD pattern probably because of the minority presence of CNT as a thin layer and the lack of long-range order in the short graphene sheets.

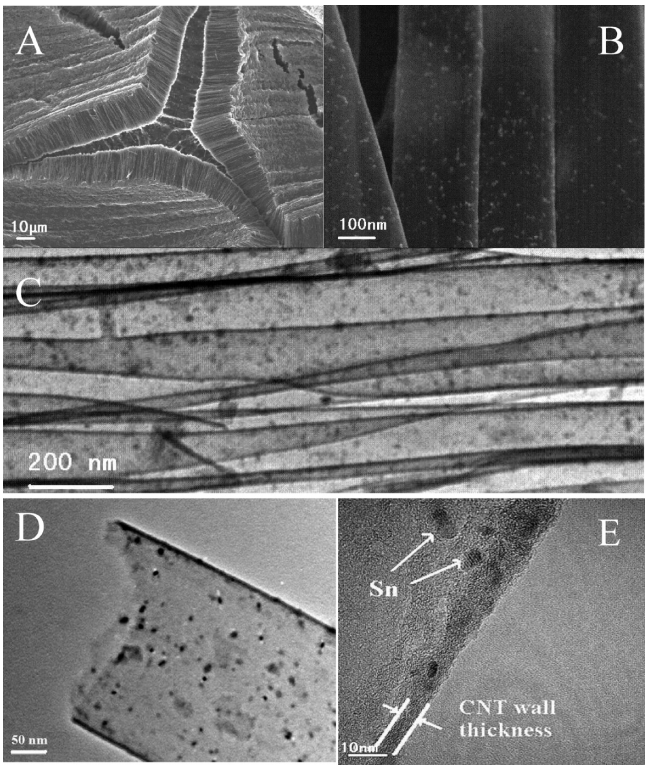

Figure 2. CNT-encapsulated Sn nanoparticles (Sn@CNT, Sample A): (a) low magnification FE-SEM image of the CNT arrays. (b) High magnification FE-SEM side view. (c,d) TEM images. (e) HRTEM image.

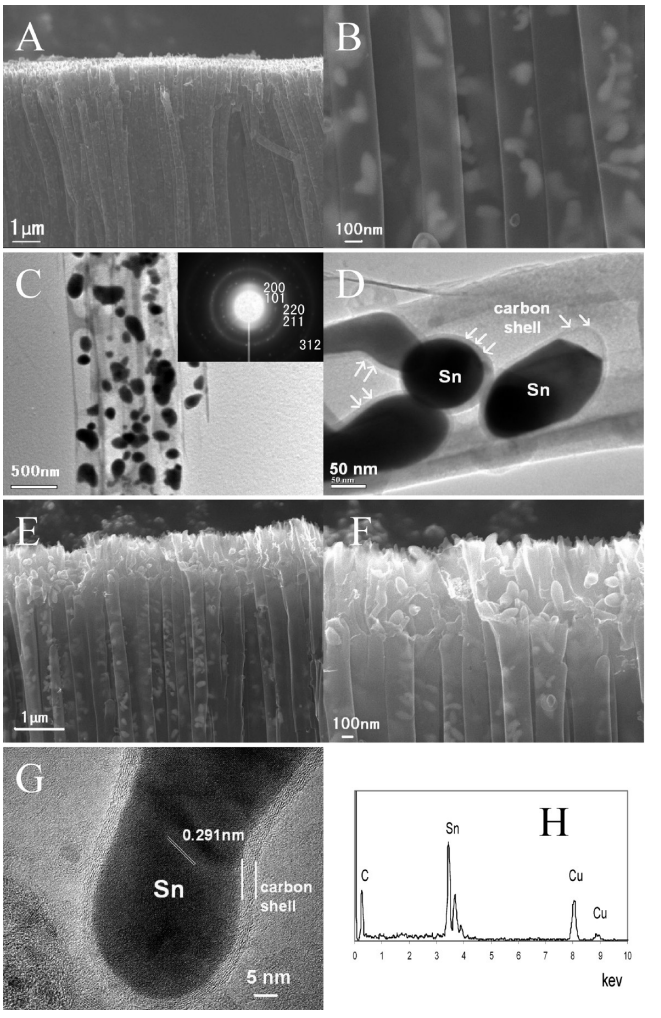

Figure 3. CNT-encapsulated Sn-carbon/core−shell particles (Sn@C@CNT, Sample B): (a, b) FE-SEM side view. (c, d) TEM images. (e, f) FE-SEM images showing the ruptured tips of Sn@C@CNT; a sand paper was used to rupture the tips of the CNTs. (g) HRTEM image showing single crystalline Sn core and amorphous carbon shell. (h) Energy dispersive X-ray spectrum (EDX) of Sn@C@CNT. The inset of (c) shows the corresponding SAED pattern of Sn.

(Figure 2e) of the smaller Sn particles of Sample A, or the layer could be too thin to be detectable. Nevertheless, as the Sn particles increased in size (Sample B), there was a comparatively larger amount of C_2H_2 decomposition and carbon deposition on the Sn particles, resulting in the formation of a relatively thick and visible carbon skin. The HRTEM image Figure 3g shows the single crystalline Sn core and the ~3 nm carbon overlayer with shortened graphene sheets which is similar to the CNT shell of Figure 2e. The energy dispersive X-ray spectrum (EDX) in Figure 3h verified the presence of Sn in the sample.

On the basis of the material characterizations we conclude that Sn nanoparticles (Sample A) and Sn@carbon core−shell particles (Sample B) were completely encapsulated by and uniformly distributed in CNTs. This is a significant improvement over previous works on CNT-encapsulated SnO[20] and CNT-encapsulated SnO_2[21,22] where Sn-based particles were also found on the CNT exterior walls or existed independently. In these studies preformed CNTs were used as the template to draw in $SnCl_2$ aqueous solution[20,21] or molten $SnCl_2$[22] by capillary

forces.[23,24] The small opening and the long CNT length rendered the filling process a difficult and tortuous one. Inevitably some precursor would also wet the CNT exterior surface and formed nanoparticles there or outside of the CNTs upon reduction. Preformed CNT templates were not used in this study. Instead the CNT templates were formed in situ on the $SnCl_4$-loaded alumina template walls by the catalytic decomposition of C_2H_2.[11,25] The slower kinetics of C_2H_2 reduction of $SnCl_4$ was exploited to form Sn nanoparticles asynchronously with CNT formation, so as to enable the complete and uniform encapsulation of the Sn nanoparticles by CNTs. C_2H_2 decomposition could also occur on larger Sn particles to form a Sn-core/carbon-shell nanostructure. Figure 4 is the schematic sketch of the perceived growth process for Sn@CNT (Sample A) and Sn@C@CNT (Sample B). It should be noted that the $SnCl_4$ aqueous solution was introduced before forming CNTs in the alumina template. Otherwise the thin layer of carbon formed on the alumina upper surface during the CNT growth would inhibit the uniform uptake of the $SnCl_4$ aqueous solution into the alumina template.

The CNT encapsulated Sn had an overall pseudohomogenous structure that minimized the contributions from heterogeneities such as isolated Sn particles or Sn nanoparticles on the CNT exterior walls. It also allowed a more unambiguous assessment of the effects of CNT encapsulation on the volume changes in the lithium storage process. From the first cycle discharge and charge curves of CNT-encapsulated Sn composites (Figure 5a) measured between 3 V and 5 mV, initial specific charge capacities of ~716 mA h g^{-1} and 526 mA h g^{-1} were calculated for Sn@C@CNT and Sn@CNT, respectively. On the basis of the simple geometrical model of a cylindrical pore, the corresponding initial volumetric capacities were estimated to be ~1489 mA h cm^{-3} and 237 mA h cm^{-3}, respectively. The first-cycle Coulombic efficiencies were 77.8% and 67.5%, respectively, but quickly improved to close to 100% in subsequent cycles for both samples. The presence of Sn in the composites also lowered the initial capacity losses relative to the case of pristine CNTs (43.7%). These values were also lower than the SnO_2 based composite anodes (~50%)[8,10] because charge consumption to activate the anode material (e.g., SnO_2 to Sn) was not required in this case. From the cycling performance of the CNT-encapsulated Sn composites shown in Figure 5b, capacity fading was still very noticeable in Sn@C@CNT despite the presence of a thin carbon overlayer on Sn. The size of the encapsulated Sn particles (~50−170 nm) was likely the cause because of the known instability of large Sn nanoparticles to cycling.[1] The carbon overlayer was not able to address the potential loss of accessibility of the larger tin particles which were more susceptible to pulverization by the repetitive lithium insertion and extraction process. Capacity fading of Sn@CNT was more subdued over the course of 80 charge and discharge cycle (Figure 5b). About 90.1% of the initial capacity could still be retained at the end of the run. Presented in another way, the capacity contribution from Sn in the nanocomposites is shown

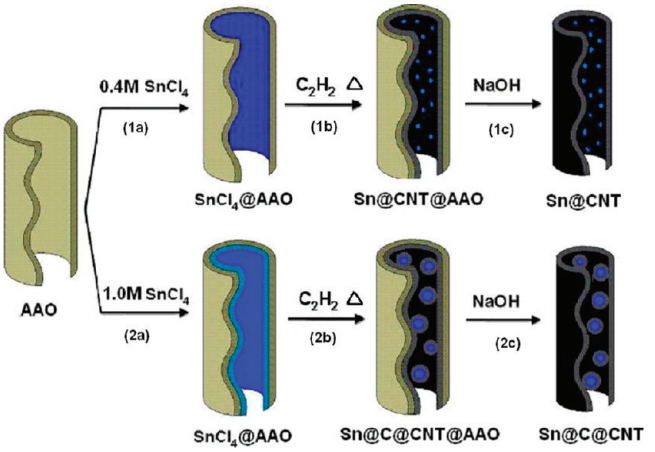

Figure 4. Schematic illustrations showing the formation of Sn@CNT and Sn@C@CNT.

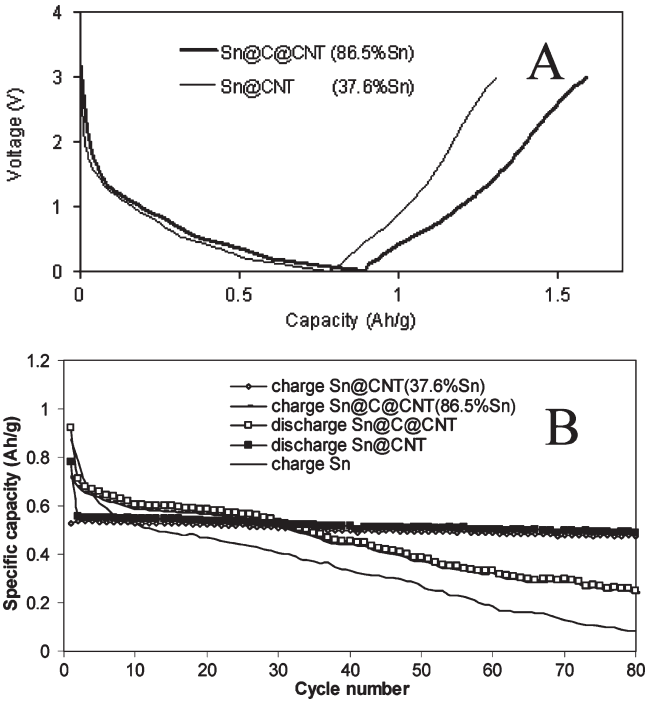

Figure 5. Electrochemical properties of CNT-encapsulated nanostructures: (a) the first-cycle discharge (Li^+ insertion) and charge curves (Li^+ extraction) of Sn@CNT and Sn@C@CNT anode (5 mV−3 V, 0.1 mA·cm^{-2}). (b) Cycling performance of Sn@CNT, Sn@C@CNT, and Sn nanoparticles[10]. Potential range: 5 mV−3 V vs Li^+/Li, current density: 0.1 mA.cm^{-2}.

in Figure 6a. For Sn@CNT with smaller encapsulated Sn particles of 6−10 nm, the contribution from Sn to the overall capacity was about 1050 mA h g^{-1} for the first 20 cycles, which is larger than the theoretical capacity of Sn (~990 mA h g^{-1}) and much higher than the capacities of Sn in Sn@C@CNT and in Sn nanoparticles[10] alone. The higher-than-theoretical capacities could be attributed to the additional storage of Li ions in the large interstitial areas formed by the stacking of nanoscale materials.[8−10,12] Figure 6b,c shows the Sn@CNT and Sn@C@CNT anodes after 80 discharging and charging cycles; the tubular structure was preserved and many small particles (~10 nm)

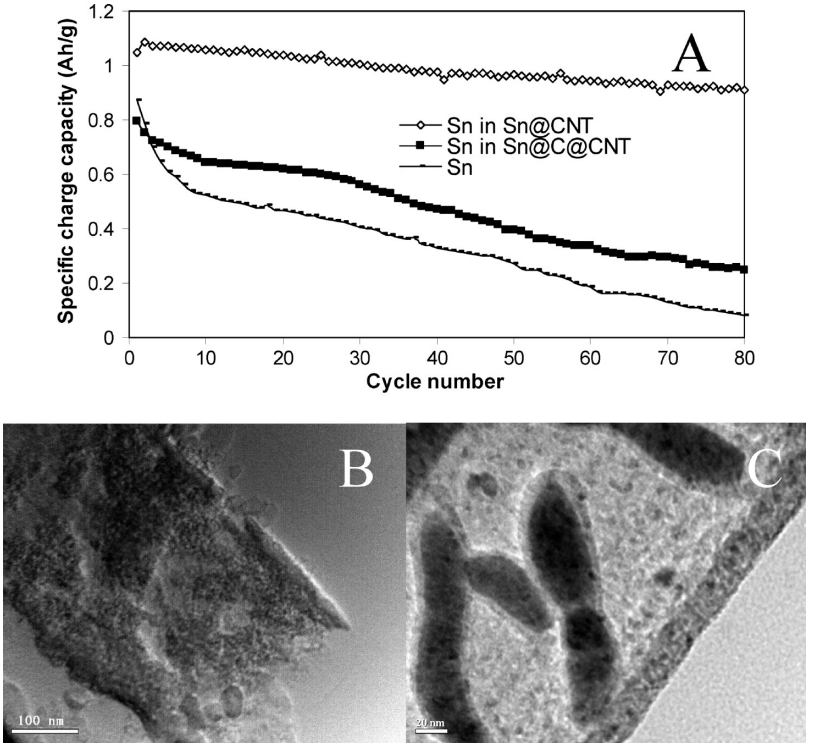

Figure 6. (a) Sn contributions in Sn@CNT and Sn@C@CNT, assuming that the CNTs contributed a constant capacity of 210 mA h g^{-1} (experimental value) throughout cycling.[11] The specific charge capacity of Sn was calculated as (composite capacity − 210 × weight fraction of CNT)/(weight fraction of Sn). (b) TEM image of Sn@CNT electrode after 80 cycles; the scattered particles around nanotubules were mixtures of carbon black and the binder chemical used for fabrication of the anodes. (c) TEM image of Sn@C@CNT electrode after 80 cycles.

could be still detected for Sn@CNT, indicating there was no significant particle growth throughout the cycling.

The cycling performance of Sn@CNT was superior to that of 6−15 nm Sn nanoparticles[10] and unencapsulated CNT−Sn composites.[18,19] The good performance could be attributed to a number of reasons arising from the complete and uniform encapsulation of small Sn nanoparticles in CNTs. First, the Sn particles were 6−10 nm in size while the CNTs were ∼200 nm in diameter, and there was ample void space in the CNTs to accommodate the volume excursion in the active Sn phase during lithium insertion and extraction reactions.[15] Second, Sn particles were uniformly distributed in a soft matrix capable of absorbing the stress induced by volume changes. The use of smaller Sn nanoparticles also reduced the nonuniform distribution of stresses. Third, complete encapsulation ensured good electrical contact between CNT and Sn. The web-like structure of the CNT matrix allowed temporarily dislocated Sn particles to be electrically reconnected again at other parts of the CNT matrix.[9] The detachment of coated Sn particles from the external surface of CNTs, on the contrary, would lead to a permanent loss of use because of the loss of electrical contact. Compared to recently reported hollow carbon-encapsulated Sn particles[13−15] and commercial Sn−Co−C,[27] the cycling performance of CNT-encapsulated Sn particles was a noteworthy improvement. The use of large-bore big CNTs (∼200 nm diameter) and good control of the Sn particle size (6−10 nm) were major contributing factors. First, CNT is a better electronic conductor, mechanically stronger and yet more flexible than the common carbon. Second, the size of the Sn particles here (6−10 nm) was only ∼1/6−1/33 of the Sn particles (60−100 or ∼200 nm) in the previous studies.[13,15] On the basis of the calculated size of the active Sn phase in a carbon matrix, there was more void space in the CNT-encapsulated Sn particles than in hollow carbon sphere-encapsulated Sn particles.[13−15] A large void space has been demonstrated to be very beneficial to buffering large volume changes in cycling.[13−15]

Conclusions

In summary, Sn particles (either as pristine Sn or Sn@carbon core−shell particles) with good control of size and morphology (6−10 nm or 50−170 nm spheres) were uniformly distributed in CNTs (∼200 nm in diameter) by a facile templated synthesis. Process-wise this represents a significant improvement over previous encapsulation efforts which captured only SnO or SnO_2 nanoparticles amidst nonspecific deposition on both the inside and the outside walls of the CNTs.[20−22] The complete and uniform encapsulation of small active Sn particles within a comparatively spacious CNT matrix ensured sufficient void space, good electrical contact, and good mechanical stability to accommodate the large volume changes in repetitive lithium insertion and extraction reactions. The CNT-encapsulated Sn nanostructure (Sn@CNT), in particular, exhibited high reversible capacity and good cyclability for a Sn-based material, making

(27) Fan, Q.; Chupas, P. J.; Whittingham, M. S. *Electrochem. Solid-State Lett.* **2007**, *10*, A274.

it suitable as an alternative anode material for lithium-ion batteries. This method of CNT encapsulation may also be useful for other high capacity Li-ion storage compounds such as Si.[28]

(28) Kim, H.; Cho, J. *Nano Lett*. **2008**, *8*, 3688.

Acknowledgment. The authors gratefully acknowledge SRF for ROCS, State Education Ministry, Shanghai Pujiang Program (07pj14042), National Natural Science Foundation of China (50701029, 20871081), and Shanghai Municipal Education Commission (S30109,08yz03,09zz96) for the financial support.